Indirect Exchange Interaction Leads to Large Lattice Contribution to Magnetocaloric Entropy Change

Lokanath Patra🄳 and Bolin Liao🄳[*]

Department of Mechanical Engineering, University of California, Santa Barbara, California 93106, USA

Materials with a large magnetocaloric response are highly desirable for magnetic cooling applications. It is suggested that a strong spin-lattice coupling tends to generate a large magnetocaloric effect, but no microscopic mechanism has been proposed. In this Letter, we use spin-lattice dynamics simulation to examine the lattice contribution to the magnetocaloric entropy change in bcc iron (Fe) and hcp gadolinium (Gd) with exchange interaction parameters determined from *ab initio* calculations. We find that indirect Ruderman-Kittel-Kasuya-Yosida (RKKY) exchange interaction in hcp Gd leads to longer-range spin-lattice coupling and more strongly influences the low-frequency long-wavelength phonons. This results in a higher lattice contribution toward the total magnetocaloric entropy change as compared to bcc Fe with short-range direct exchange interactions. Our analysis provides a framework for understanding the magnetocaloric effect in magnetic materials with strong spin-lattice couplings. Our finding suggests that long-range indirect RKKY-type exchange gives rise to a larger lattice contribution to the magnetocaloric entropy change and is, thus, beneficial for magnetocaloric materials.

Introduction.—Magnetic refrigeration is based on the magnetocaloric effect (MCE), which is the material's ability to heat (cool) when magnetized (demagnetized) in an adiabatic process [1–4]. The MCE originates from the magnetic order-disorder transition induced by an external magnetic field and the associated entropy change. Understanding and designing materials with a strong MCE are of both great scientific and technological importance. Fundamentally, MCE provides a convenient probe to examine the interplay between magnetism and other excitations in condensed matter systems [5,6]. Technologically, MCE has been widely adopted to obtain cryogenic temperatures in space missions [7], observatory astronomy [8], and scientific experimentation [9], where compact and reliable cooling solutions are required. Magnetic refrigeration near room temperature has also been considered as an environmentally friendly alternative to conventional refrigeration based on vapor compression cycles [10]. MCE materials can be characterized by the isothermal entropy change ΔS, which measures the change in the equilibrium entropy of a material as a result of an externally applied magnetic field. Under isothermal conditions, the entropy change ΔS manifests itself as the amount of heat released or absorbed by the material when an external magnetic field is applied or removed. Therefore, ΔS is a metric for the cooling capacity of an MCE material.

Magnetocaloric materials with a strong coupling between spin and lattice degrees of freedom are known to exhibit a large MCE. Prominent examples are the first-order MCE materials, where the magnetic transition is associated with a first-order structural phase transition [11–13]. The observed large MCE is governed by the concurrent magnetic and structural phase transition as a result of the strong spin-lattice coupling since the applied magnetic field can simultaneously change the magnetic and lattice entropy in these materials. The lattice contribution to the entropy change ΔS_L has been reported to be 50%–60% or more of the total entropy change in the materials undergoing a magnetostructural or magnetoelastic transition [14–16]. Even in conventional second-order MCE materials, a strong spin-lattice coupling is usually an indicator of a strong MCE [17]. Earlier efforts to isolate the lattice contribution to the magnetocaloric entropy change were based on either empirical assumptions (e.g., the lattice contribution is proportional to magnetostriction [18]) or mean field theories with empirical parameters [19,20]. More recently, the combination of first-principles calculation based on density functional theory (DFT) and statistical models has enabled evaluations of the lattice contribution in several materials [21–24]. These studies enhanced our understanding of the interplay between lattice dynamics and magnetic entropy but did not reveal the origin of the large lattice contribution to the entropy change, and an atomic-level understanding of the relationship between spin-lattice coupling and the MCE is currently lacking. In particular, it is unclear what microscopic mechanisms are responsible for the strong spin-lattice coupling and the associated high MCE. In this light, atomistic computational methods to quantify the entropy

contributions from the spin and the lattice degrees of freedom separately are of pivotal importance for the discovery and optimization of the MCE materials.

The isothermal entropy change in magnetocaloric materials can be calculated from their magnetizations as functions of temperature and applied magnetic field, following the thermodynamic Maxwell relation [1]:

$$\Delta S(T, \Delta H) = \mu_0 \int_{H_i}^{H_f} \left(\frac{\partial M(T,H)}{\partial T} \right)_H dH, \quad (1)$$

where $\Delta H = H_f - H_i$ is the change of the applied external field (H_f and H_i are final and initial fields, respectively), μ_0 is the Bohr magneton, M is the magnetization, and T is the temperature. The field- and temperature-dependent magnetization can be obtained by simulating the dynamics of atomic spins in magnetic materials using atomic spin dynamics (ASD) simulations with magnetic exchange interaction parameters (J_{ij}, where i and j label the interacting spins) calculated from *ab initio* methods [25–27]. However, these simulations ignore the effect of thermal fluctuations of the atoms (lattice vibrations) at finite temperatures and, thus, cannot capture the spin-lattice coupling effect and the resultant lattice contribution to the magnetocaloric entropy change (ΔS_L). Hence, ASD simulations need to be modified to account for the lattice vibrations and explicitly include the dependence of the spin exchange interactions on the dynamical lattice positions in order to simulate the dynamics of materials with strong spin-lattice coupling [28,29]. For this purpose, spin-lattice dynamics (SLD) simulations add the lattice dynamics and the lattice-dependent spin exchange interactions to the ASD simulations and have been reported to be an effective tool to predict magnetic and thermodynamic properties of magnetic materials more accurately [30–33]. However, SLD simulations have not been applied to analyze the spin and lattice contributions to the magnetocaloric entropy change thus far.

In the current study, we use SLD simulations to quantify the spin and lattice contributions to the magnetocaloric entropy change with a particular focus on understanding the effect of different types of magnetic exchange interactions on MCE. For this purpose, we carry out a thorough comparison between two representative direct and indirect exchange materials, body-centered-cubic (bcc) Fe and hexagonal-closed-pack (hcp) Gd, respectively [34]. In magnetic materials with direct exchange interactions, such as bcc Fe, the magnetic exchange interactions are mediated directly by spin-polarized conduction electrons near the Fermi level. In this case, the strength of the direct exchange interaction decreases rapidly with the distance between magnetic ions. In contrast, indirect exchange interactions can couple magnetic moments over relatively large distances [35]. Ruderman-Kittel-Kasuya-Yosida (RKKY) interaction is a particular form of indirect magnetic exchange interaction that is dominant in metals with little

or no direct overlap between neighboring magnetic electrons [36]. Instead, the exchange interactions between magnetic ions are mediated by conduction electrons. hcp Gd is an archetypal example of the RKKY interaction [37–39]. The RKKY interaction features an oscillating interaction strength with a periodicity determined by the Fermi wave vector that can lead to longer-range interactions between magnetic ions [40]. With detailed SLD simulations of bcc Fe and hcp Gd, we demonstrate that longer-range RKKY interactions can lead to stronger spin-lattice coupling affecting low-frequency and long-wavelength phonons, which gives rise to a much higher contribution from the lattice to the magnetocaloric entropy change. Our study provides a microscopic mechanism for the enhancement of MCE via spin-lattice coupling and suggests that RKKY interaction is a preferable type of exchange interaction when searching for materials with a strong MCE. We note that, since the electronic contribution to the magnetocaloric entropy change is negligible in hcp Gd [22], the electronic entropy contribution is not discussed in this Letter.

Results and discussions.—Details of the computational methods are provided in the Supplemental Material (SM) [41]. The spin-dependent electron density of states (DOS) of bcc Fe and hcp Gd is shown in Fig. S1 in the SM. In bcc Fe, the conducting d electrons near the Fermi level are spin polarized and are responsible for the direct exchange interactions. In contrast, in hcp Gd, the conducting electrons near the Fermi level are not spin polarized while the magnetism comes from the deep f electrons. In this case, the conducting electrons mediate the RKKY interactions. The magnetic exchange parameters (J_{ij}) as a function of interatomic distance (R_{ij}) for bcc Fe are given in Fig. 1(a). In bcc Fe, J_{ij} is short-ranged as it decreases
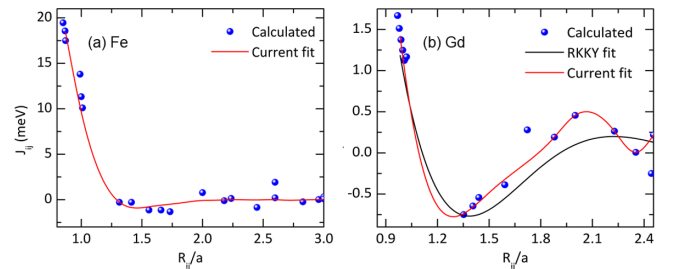

FIG. 1. Comparison of direct exchange and RKKY exchange interactions in bcc Fe and hcp Gd. Exchange coupling constants J_{ij} as a function of interatomic distance (R_{ij}/a, where a is the lattice constant) between atoms i and j for (a) bcc Fe and (b) hcp Gd. "Current fit" refers to analytical Bethe-Slater equations [Eq. (S4) in the SM [41]] fitted to the calculated exchange interaction parameters. "RKKY fit" in (b) refers to the analytical RKKY equation [Eq. (S5) in the SM] fitted to the calculated exchange interaction parameters in hcp Gd. The exchange interaction in bcc Fe decays rapidly and is, thus, short-ranged. In contrast, the exchange interaction in hcp Gd shows an oscillatory behavior and decays more slowly with distance.

rapidly with distance and the values are smaller by at least an order of magnitude after the first two nearest neighbor interactions. The calculated exchange parameters have similar values as reported by previous studies [50–53]. The calculated J_{ij} values were fitted to the Bethe-Slater equation [Eq. (S4) in the SM] to analyze the behavior as a function of interatomic distance, as shown in Fig. 1(a).

The behavior of J_{ij} as a function of interatomic distance in hcp Gd is quite different as compared to that in bcc Fe. Despite the fact that Gd is ferromagnetic at a lower temperature, many of the exchange constants are antiferromagnetic. The dependence of the magnetic exchange parameters on the interatomic distance [Fig. 1(b)] reveals an oscillatory behavior between ferromagnetism and antiferromagnetism as the interatomic distance grows. This is characteristic of the RKKY exchange [36,54,55]. The exchange parameters within the first ten nearest neighbors were considered for further calculations, beyond which the interaction strength becomes negligible. Unlike the transition metals, the large magnetic moment ($\sim 7.5\mu_B$ per atom) and strongly correlated behavior of rare-earth hcp Gd originated from half-filled $4f$ shells. Because of the strong localization of these orbitals, the overlap between neighboring atomic sites is dominated by the $6s$, $6p$, and $5d$ states [56]. The direct exchange contribution from the $4f$ orbital has been found to be small and antiferromagnetic and hence does not affect the magnetic ordering significantly [57]. The simulated J_{ij} values for hcp Gd agree well with previously reported computational and experimental values [39,58,59]. The calculated RKKY-type J_{ij} values were fitted with piecewise Bethe-Slater curves using different cutoff radii, as shown in Fig. 1(b). The details of the fitting process are given in the SM [41]. The fitted analytical Bethe-Slater equations were used to evaluate distance-dependent exchange interactions in the SLD simulation.

The calculated J_{ij} values were used to simulate the Curie temperatures (T_C) of bcc Fe and hcp Gd using ASD as well as SLD simulations. Notably, the Dudarev-Derlet embedded atom method interatomic potenial [60] was used for the SLD simulation of bcc Fe to capture the itinerant nature of the $3d$ electrons. The resulting magnetization versus temperature curves are displayed in Figs. 2(a) and 2(b). The results were then fitted to a simple power-law decay function of the form $M(T) = [1 - (T/T_C)]^\beta$, where M is the magnetization and β is the critical exponent. The fitted T_C values with the static-lattice-based ASD approach are 1180 and 330 K for bcc Fe and hcp Gd, respectively, and in fair agreement with experimental measurements. However, ASD simulations are not adequate for quantitative studies of materials with spin-lattice coupling [30]. The lattice effect in the description of the finite-temperature magnetism in bcc Fe and hcp Gd has been done recently [27]. Incorporating the lattice dynamics into effect, our SLD simulations predicted the T_C to be 1060 and 310 K,
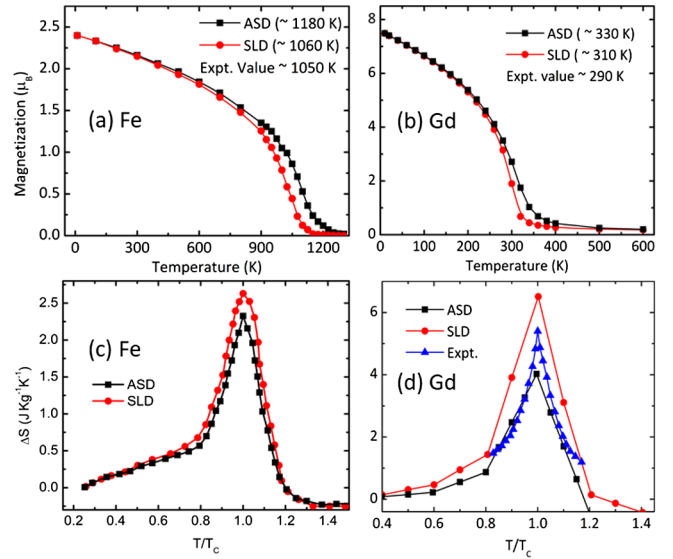

FIG. 2. ASD and SLD simulation of the Curie temperature and isothermal entropy change in bcc Fe and hcp Gd. The simulated magnetization as a function of temperature is shown for (a) bcc Fe and (b) hcp Gd using both ASD and SLD. The total isothermal entropy changes (ΔS) are shown for (c) bcc Fe and (d) hcp Gd calculated using both ASD and SLD methods for a field change of 2 T. The T_C and ΔS values are provided and compared with the experimentally measured values when available. Including lattice dynamics and spin-lattice coupling leads to a better agreement with experimental values. We did not find available experimental ΔS data for bcc Fe.

respectively, for bcc Fe and hcp Gd, with better agreements with the experimentally measured values.

To understand the difference between the magnetocaloric responses of materials with direct and indirect RKKY exchange coupling parameters, we calculated the isothermal entropy changes with both ASD and SLD simulations for bcc Fe [Fig. 2(c)] and hcp Gd [Fig. 2(d)]. The external-field-dependent magnetization versus temperature curves were simulated (Figs. S2 and S4 in the SM [41]) and the entropy changes were evaluated using Eq. (1). The calculated total entropy change of bcc Fe and hcp Gd as a function of temperature and external magnetic field using SLD is shown in Figs. S3 and S5 in the SM. The total entropy change of bcc Fe was calculated to be 2.33 and 2.63 $J\,kg^{-1}\,K^{-1}$ with ASD and SLD simulations, respectively, for a magnetic field change of 2 T. We did not find experimental entropy change values in bcc Fe to benchmark our simulation. However, the adiabatic temperature change estimated (Fig. S6 in the SM [41]) based on our simulated entropy change and the experimental specific heat of bcc Fe [61] is in good agreement with early measurements [62]. The difference between the entropy change values obtained from ASD and SLD simulations (0.3 $J\,kg^{-1}\,K^{-1}$) can be attributed to the lattice contribution to the isothermal entropy change at the transition temperature, which amounts to 13% of the pure spin contribution

from the ASD simulation. Next, we analyze the effect of indirect RKKY exchange on the isothermal entropy change in hcp Gd using similar approaches. The evaluated isothermal entropy change using the spin-only Hamiltonian through the ASD simulation is $\sim$4.1 J kg^{-1} K^{-1} for a magnetic field change of 2 T. This calculated value based on ASD is smaller compared to the experimentally measured value of $\sim$5.4 J kg^{-1} K^{-1} [63]. The sizable discrepancy suggests that the missing lattice dynamics in the ASD simulation can be significant in indirect RKKY exchange materials such as hcp Gd. To verify this hypothesis, we performed SLD simulations of hcp Gd using the interatomic potential developed by Baskes and Johnson [64] and an isothermal entropy change of $\sim$6.3 J kg^{-1} K^{-1} was predicted. This result suggests a lattice entropy contribution of 2.2 J kg^{-1} K^{-1} for a magnetic field change of 2 T, which is 53.6% of the pure spin contribution. Our findings agree with Martinho Vieira *et al.* [22]. The SLD-evaluated total entropy change is higher than the measured value by 0.9 J kg^{-1} K^{-1}, which can be potentially attributed to the sample purity and measurement uncertainty in the experiment, as well as the uncertainty of certain computational parameters, such as the "U" parameter used in our DFT $+ U$ calculation (details in the SM [41]).

The significant lattice entropy change with an applied magnetic field indicates a stronger magnon-phonon coupling in indirect RKKY-exchange-based materials. Microscopically, this result suggests that the phonon structure in hcp Gd near the Curie temperature is sensitively tuned by the external magnetic field. Therefore, it is informative to explicitly examine the phonon dispersion relation of hcp Gd as influenced by an external magnetic field to determine which phonon modes are mostly affected by the applied field. For this purpose, the frequencies of the phonon modes were calculated by solving the dynamic matrix elements obtained from the lattice Green's functions that can be directly calculated from the atomic trajectories in the SLD simulation [65]. Figure 3 shows the phonon dispersions of bcc Fe and hcp Gd calculated with magnetic fields of 0 and 5 T, respectively. As seen from Fig. 3(a), in bcc Fe, significant changes in the phonon dispersion can only be noticed at higher phonon frequency ranges ($>$3 THz) and near the Brillouin zone boundaries, whereas the low-frequency and long-wavelength phonons remain unaffected. This feature is more clearly shown in the phonon density of states shown in Fig. 3(b). This observation can be understood as follows. Since the spin-lattice coupling originates from the dependence of the magnetic exchange parameters on the interatomic distance (dJ_{ij}/dR_{ij}), the rapidly decreasing J_{ij} as a function of R_{ij} in direct exchange materials [such as bcc Fe, as shown in Fig. 1(a)] determines that the spin-lattice coupling mainly affects the short-wavelength lattice vibrations, with a wavelength on the order of the range of the direct exchange. These short-wavelength phonons usually reside near the
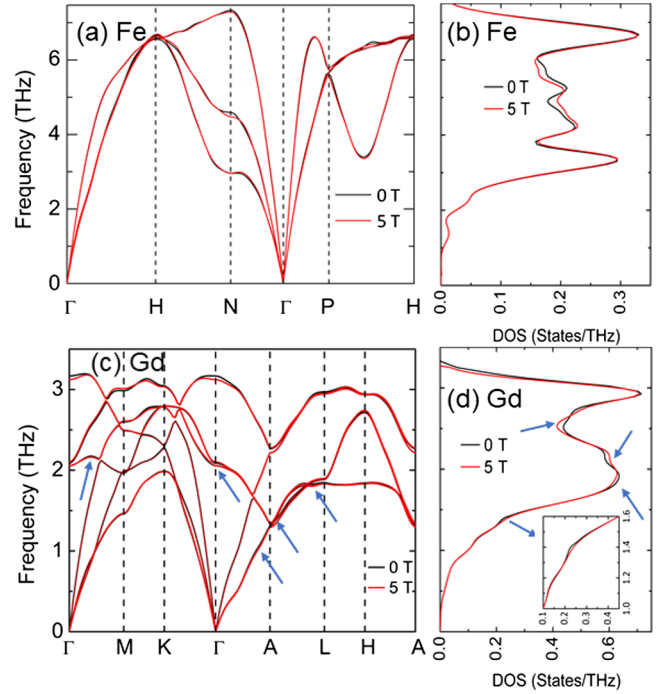

FIG. 3. External-magnetic-field-dependent phonon spectra and density of states (DOS). Simulated phonon spectra and DOS in (a),(b) bcc Fe and (c),(d) hcp Gd at 0 and 5 T with the SLD approach. The changes in low-frequency phonons for hcp Gd are indicated with arrow marks. The magnetic field has a stronger influence on low-frequency and long-wavelength phonons in hcp Gd.

Brillouin zone boundary and within the higher-frequency range, so their occupation is lower at a given temperature, leading to a smaller contribution to the entropy change. In contrast, the phonon dispersion of hcp Gd, as shown in Fig. 3(c), shows noticeable changes in lower-frequency and longer-wavelength ranges, as labeled by the arrows in Fig. 3(c), indicating that the spin-lattice coupling in hcp Gd occurs on a larger length scale. This is consistent with the oscillatory behavior of the magnetic exchange parameters as a result of the indirect RKKY exchange interaction, as shown in Fig. 1(b). Although the overall magnetic exchange strength in hcp Gd is weaker than that in bcc Fe, which leads to a lower Curie temperature in hcp Gd, the much slower decay of the magnetic exchange parameters and their oscillatory behavior as a function of distance leads to significant (dJ_{ij}/dR_{ij}) at longer distances. As a result of this long-range spin-lattice coupling, lattice vibrations associated with phonons with longer wavelengths are more affected by the external field, which can also be seen in the field-dependent phonon density of states shown in Fig. 3(d). Since these phonons have lower frequencies and, thus, higher occupation numbers at a given temperature, they contribute more to the field-induced isothermal entropy change.

To compare the lattice entropy contribution from different phonon modes in bcc Fe and hcp Gd more clearly,

we further evaluated the lattice entropy change directly based on the field-dependent phonon dispersions. The vibrational entropy of a particular phonon mode with frequency ω in a harmonic crystal is given by the standard formula for noninteracting bosons [66]:

$$S_{\text{ph}}(\omega, T) = k_B[(n+1)\ln(n+1) - n \ln n], \quad (2)$$

where k_B is the Boltzmann constant and n is the occupation number of this phonon mode. Although this result is only rigorously true in harmonic crystals, it has been shown that [67], to the leading order in perturbation theory, Eq. (2) is still valid in anharmonic crystals as long as the renormalized phonon frequencies are used. In our case, the phonon frequencies extracted from the SLD simulation include the full renormalization effect due to both anharmonic phonon-phonon interactions and spin-lattice interactions. Using Eq. (2), the calculated total lattice entropy change from the field-dependent phonon dispersions for a field change of 2 T is $0.65 \, \text{J kg}^{-1} \, \text{K}^{-1}$ for bcc Fe and $2.5 \, \text{J kg}^{-1} \, \text{K}^{-1}$ for hcp Gd. These values are similar to those evaluated by comparing the ASD and SLD simulations, as shown in Figs. 2(c) and 2(d). To further contrast the effects of direct exchange and indirect RKKY exchange interactions on lattice entropy changes, the accumulated contribution to the total lattice entropy change from phonons with different frequencies in bcc Fe and hcp Gd under a field change of 2 T is shown in Fig. 4. As clearly seen in Fig. 4, the lower-frequency phonons have negligible contributions toward the lattice entropy change in bcc Fe,

whereas, in hcp Gd, the lower-frequency phonons have a significant contribution toward the lattice entropy change. This result confirms that the indirect RKKY-type exchange in hcp Gd can impact the short- as well as long-wavelength phonons due to its long interaction range, while the direct exchange in bcc Fe is short-ranged and can only affect the short-wavelength phonons. We note that the strong spin-lattice coupling in hcp Gd is also reflected in other phonon-related properties of Gd, for example, the strong magnetic field effect on its elastic moduli and ultrasonic attenuation [68,69] and the minimum in its thermal conductivity near the Curie temperature [70,71]. Our analysis provides a microscopic mechanism of how indirect RKKY exchange can lead to longer-range spin-lattice coupling and a significantly enhanced lattice contribution to the isothermal magnetocaloric entropy change.

Conclusion.—In summary, we applied SLD simulation to directly evaluate the spin and lattice contributions to the isothermal magnetocaloric entropy change in bcc Fe and hcp Gd. Based on a detailed analysis of the field-dependent phonon properties, we conclude that the indirect RKKY-type exchange in hcp Gd leads to a long-range spin-lattice coupling that affects long-wavelength and low-frequency phonons and, thus, causes an enhanced lattice contribution to the total entropy change. Our Letter provides a microscopic picture of how different types of spin-lattice coupling can give rise to distinct magnetocaloric responses and suggests that indirect RKKY exchange interactions are more desirable for a large MCE response, potentially guiding the future search for more efficient MCE materials.
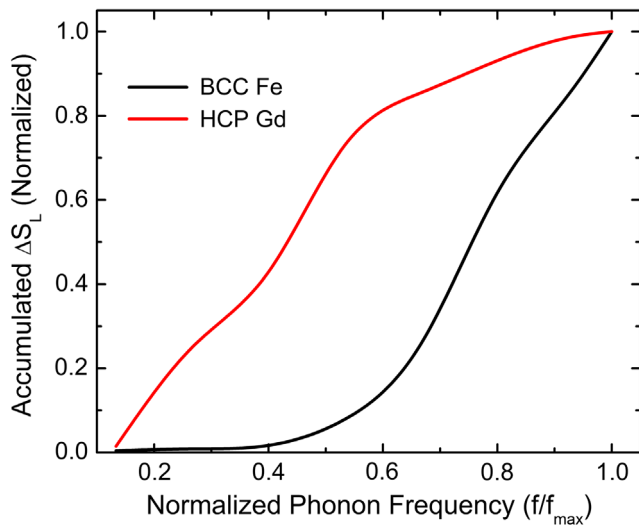
FIG. 4. Accumulated contribution to the total lattice entropy change from phonon modes as a function of phonon frequency in bcc Fe and hcp Gd. The phonon frequency is normalized to the maximum phonon frequency in either material. The accumulated contribution is also normalized to the total lattice entropy change. The entropy change is evaluated with a magnetic field of 2 T. It is clearly shown that lower-frequency phonons in hcp Gd have a much more significant contribution than those in bcc Fe.

*bliao@ucsb.edu

[1] V. K. Pecharsky and K. A. Gschneidner, Jr., Magnetocaloric effect and magnetic refrigeration, J. Magn. Magn. Mater. **200,** 44 (1999).

[2] M. Balli, S. Jandl, P. Fournier, and A. Kedous-Lebouc, Advanced materials for magnetic cooling: Fundamentals and practical aspects, Appl. Phys. Rev. 4, 021305 (2017).

[3] B. Shen, J. Sun, F. Hu, H. Zhang, and Z. Cheng, Recent progress in exploring magnetocaloric materials, Adv. Mater. 21, 4545 (2009).

[4] V. Franco, J. Blázquez, J. Ipus, J. Law, L. Moreno-Ramírez, and A. Conde, Magnetocaloric effect: From materials research to refrigeration devices, Prog. Mater. Sci. 93, 112 (2018).

[5] C. Balz, P. Lampen-Kelley, A. Banerjee, J. Yan, Z. Lu, X. Hu, S. M. Yadav, Y. Takano, Y. Liu, D. A. Tennant et al., Finite field regime for a quantum spin liquid in α-RuCl$_3$, Phys. Rev. B 100, 060405(R) (2019).

[6] P. Czajka, T. Gao, M. Hirschberger, P. Lampen-Kelley, A. Banerjee, J. Yan, D. G. Mandrus, S. E. Nagler, and N. Ong, Oscillations of the thermal conductivity in the spin-liquid state of α-RuCl$_3$, Nat. Phys. 17, 915 (2021).

[7] P. J. Shirron, M. O. Kimball, D. J. Fixsen, A. J. Kogut, X. Li, and M. J. DiPirro, Design of the PIXIE adiabatic demagnetization refrigerators, Cryogenics 52, 140 (2012).

[8] R. D. Britt and P. Richards, An adiabatic demagnetization refrigerator for infrared bolometers, Int. J. Infrared Millim. Waves 2, 1083 (1981).

[9] T. J. Sato, D. Okuyama, and H. Kimura, Tiny adiabatic-demagnetization refrigerator for a commercial superconducting quantum interference device magnetometer, Rev. Sci. Instrum. 87, 123905 (2016).

[10] C. Aprea, A. Greco, A. Maiorino, and C. Masselli, Magnetic refrigeration: An eco-friendly technology for the refrigeration at room temperature, J. Phys. Conf. Ser. 655, 012026 (2015).

[11] V. K. Pecharsky and K. A. Gschneidner, Jr., Giant Magnetocaloric Effect in Gd$_5$(Si$_2$Ge$_2$), Phys. Rev. Lett. 78, 4494 (1997).

[12] C. Magen, Z. Arnold, L. Morellon, Y. Skorokhod, P. A. Algarabel, M. R. Ibarra, and J. Kamarad, Pressure-Induced Three-Dimensional Ferromagnetic Correlations in the Giant Magnetocaloric Compound Gd$_5$Ge$_4$, Phys. Rev. Lett. 91, 207202 (2003).

[13] H. Wada and Y. Tanabe, Giant magnetocaloric effect of MnAs$_{1-x}$Sb$_x$, Appl. Phys. Lett. 79, 3302 (2001).

[14] V. K. Pecharsky, A. P. Holm, K. A. Gschneidner, Jr., and R. Rink, Massive Magnetic-Field-Induced Structural Transformation in Gd$_5$Ge$_4$ and the Nature of the Giant Magnetocaloric Effect, Phys. Rev. Lett. 91, 197204 (2003).

[15] L. Morellon, Z. Arnold, C. Magen, C. Ritter, O. Prokhnenko, Y. Skorokhod, P. A. Algarabel, M. R. Ibarra, and J. Kamarad, Pressure Enhancement of the Giant Magnetocaloric Effect in Tb$_5$Si$_2$Ge$_2$, Phys. Rev. Lett. 93, 137201 (2004).

[16] H. Wada, S. Matsuo, and A. Mitsuda, Pressure dependence of magnetic entropy change and magnetic transition in MnAs$_{1-x}$Sb$_x$, Phys. Rev. B 79, 092407 (2009).

[17] J. D. Bocarsly, E. E. Levin, C. A. Garcia, K. Schwennicke, S. D. Wilson, and R. Seshadri, A simple computational proxy for screening magnetocaloric compounds, Chem. Mater. 29, 1613 (2017).

[18] A. Aliev, A. Batdalov, and L. Khanov, Magnetic and lattice contributions to the magnetocaloric effect in Sm$_{1-x}$Sr$_x$MnO$_3$ manganites, Appl. Phys. Lett. 112 (2018).

[19] B. P. Alho, P. O. Ribeiro, P. J. von Ranke, F. Guillou, Y. Mudryk, and V. K. Pecharsky, Free-energy analysis of the nonhysteretic first-order phase transition of Eu$_2$In, Phys. Rev. B 102, 134425 (2020).

[20] P. Hu, J. Gong, Z. Zhang, C. Zhang, H. Wang, P. Cheng, and D. Wang, Magnetic field-dependent lattice entropy change in Gd$_5$Ge$_4$, J. Magn. Magn. Mater. 566, 170306 (2023).

[21] R. M. Vieira, O. Eriksson, A. Bergman, and H. C. Herper, High-throughput compatible approach for entropy estimation in magnetocaloric materials: Ferh as a test case, J. Alloys Compd. 857, 157811 (2021).

[22] R. Martinho Vieira, O. Eriksson, T. Björkman, A. Bergman, and H. C. Herper, Realistic first-principles calculations of the magnetocaloric effect: Applications to hcp Gd, Mater. Res. Lett. 10, 156 (2022).

[23] B. Li, W. Ren, Q. Zhang, X. Lv, X. Liu, H. Meng, J. Li, D. Li, and Z. Zhang, Magnetostructural coupling and magnetocaloric effect in Ni–Mn–In, Appl. Phys. Lett. 95, 172506 (2009).

[24] R. Korotana, G. Mallia, N. Fortunato, J. Amaral, Z. Gercsi, and N. Harrison, A combined thermodynamics and first principles study of the electronic, lattice, and magnetic contributions to the magnetocaloric effect in La$_{0.75}$Ca$_{0.25}$MnO$_3$, J. Phys. D 49, 285001 (2016).

[25] V. P. Antropov, M. I. Katsnelson, M. van Schilfgaarde, and B. N. Harmon, Ab Initio Spin Dynamics in Magnets, Phys. Rev. Lett. 75, 729 (1995).

[26] B. Skubic, J. Hellsvik, L. Nordström, and O. Eriksson, A method for atomistic spin dynamics simulations: Implementation and examples, J. Phys. Condens. Matter 20, 315203 (2008).

[27] P.-W. Ma and S. L. Dudarev, Dynamic magnetocaloric effect in bcc iron and hcp gadolinium, Phys. Rev. B 90, 024425 (2014).

[28] V. Pecharsky, K. Gschneidner, Jr., Y. Mudryk, and D. Paudyal, Making the most of the magnetic and lattice entropy changes, J. Magn. Magn. Mater. 321, 3541 (2009).

[29] A. Aliev, L. Khanov, A. Gamzatov, A. Batdalov, D. Kurbanova, K. Yanushkevich, and G. Govor, Giant magnetocaloric effect in MnAs$_{1-x}$P$_x$ in a cyclic magnetic field: Lattice and magnetic contributions and degradation of the effect, Appl. Phys. Lett. 118, 072404 (2021).

[30] P.-W. Ma, C. H. Woo, and S. L. Dudarev, Large-scale simulation of the spin-lattice dynamics in ferromagnetic iron, Phys. Rev. B 78, 024434 (2008).

[31] X. Wu, Z. Liu, and T. Luo, Magnon and phonon dispersion, lifetime, and thermal conductivity of iron from spin-lattice dynamics simulations, J. Appl. Phys. 123, 085109 (2018).

[32] J. Hellsvik, D. Thonig, K. Modin, D. Iuşan, A. Bergman, O. Eriksson, L. Bergqvist, and A. Delin, General method for atomistic spin-lattice dynamics with first-principles accuracy, Phys. Rev. B 99, 104302 (2019).

[33] D. Perera, D. M. Nicholson, M. Eisenbach, G. M. Stocks, and D. P. Landau, Collective dynamics in atomistic models with coupled translational and spin degrees of freedom, Phys. Rev. B 95, 014431 (2017).

[34] W. Nolting and A. Ramakanth, *Quantum Theory of Magnetism* (Springer Science & Business Media, New York, 2009).

[35] S. S. P. Parkin, Systematic Variation of the Strength and Oscillation Period of Indirect Magnetic Exchange Coupling through the 3d, 4d, and 5d Transition Metals, Phys. Rev. Lett. **67**, 3598 (1991).

[36] M. A. Ruderman and C. Kittel, Indirect exchange coupling of nuclear magnetic moments by conduction electrons, Phys. Rev. **96**, 99 (1954).

[37] P.-A. Lindgård, B. Harmon, and A. Freeman, Theoretical Magnon Dispersion Curves for Gd, Phys. Rev. Lett. **35**, 383 (1975).

[38] A. T. Hindmarch and B. J. Hickey, Direct Experimental Evidence for the Ruderman-Kittel-Kasuya-Yosida Interaction in Rare-Earth Metals, Phys. Rev. Lett. **91**, 116601 (2003).

[39] A. Scheie, P. Laurell, P. A. McClarty, G. E. Granroth, M. B. Stone, R. Moessner, and S. E. Nagler, Spin-exchange Hamiltonian and topological degeneracies in elemental gadolinium, Phys. Rev. B **105**, 104402 (2022).

[40] S. S. P. Parkin, N. More, and K. P. Roche, Oscillations in Exchange Coupling and Magnetoresistance in Metallic Superlattice Structures: Co/Ru, Co/Cr, and Fe/Cr, Phys. Rev. Lett. **64**, 2304 (1990).

[41] See Supplemental Material at http://link.aps.org/supplemental/10.1103/PhysRevLett.131.066703 for the details regarding the DFT and spin dynamic simulations, which includes Refs. [42–49].

[42] G. Kresse and J. Furthmüller, Efficient iterative schemes for *ab initio* total-energy calculations using a plane-wave basis set, Phys. Rev. B **54**, 11169 (1996).

[43] P. E. Blöchl, Projector augmented-wave method, Phys. Rev. B **50**, 17953 (1994).

[44] J. D. Pack and H. J. Monkhorst, "Special points for Brillouin-zone integrations"—A reply, Phys. Rev. B **16**, 1748 (1977).

[45] S. L. Dudarev, G. A. Botton, S. Y. Savrasov, C. Humphreys, and A. P. Sutton, Electron-energy-loss spectra and the structural stability of nickel oxide: An LSDA + U study, Phys. Rev. B **57**, 1505 (1998).

[46] A. Belozerov and V. Anisimov, Coulomb interaction parameters in bcc iron: An LDA + DMFT study, J. Phys. Condens. Matter **26**, 375601 (2014).

[47] H. Ebert, D. Koedderitzsch, and J. Minar, Calculating condensed matter properties using the KKR-Green's function method—Recent developments and applications, Rep. Prog. Phys. **74**, 096501 (2011).

[48] J. Tranchida, S. J. Plimpton, P. Thibaudeau, and A. P. Thompson, Massively parallel symplectic algorithm for coupled magnetic spin dynamics and molecular dynamics, J. Comput. Phys. **372**, 406 (2018).

[49] S. Plimpton, Fast parallel algorithms for short-range molecular dynamics, J. Comput. Phys. **117**, 1 (1995).

[50] H. Wang, P.-W. Ma, and C. H. Woo, Exchange interaction function for spin-lattice coupling in bcc iron, Phys. Rev. B **82**, 144304 (2010).

[51] M. Pajda, J. Kudrnovský, I. Turek, V. Drchal, and P. Bruno, *Ab initio* calculations of exchange interactions, spin-wave stiffness constants, and Curie temperatures of Fe, Co, and Ni, Phys. Rev. B **64**, 174402 (2001).

[52] O. Mryasov, A. J. Freeman, and A. Liechtenstein, Theory of non-Heisenberg exchange: Results for localized and itinerant magnets, J. Appl. Phys. **79**, 4805 (1996).

[53] S. Frota-Pessôa, R. B. Muniz, and J. Kudrnovský, Exchange coupling in transition-metal ferromagnets, Phys. Rev. B **62**, 5293 (2000).

[54] T. Kasuya, A theory of metallic ferro- and antiferromagnetism on Zener's model, Prog. Theor. Phys. **16**, 45 (1956).

[55] K. Yosida, Magnetic properties of Cu-Mn alloys, Phys. Rev. **106**, 893 (1957).

[56] P. Kurz, G. Bihlmayer, and S. Blügel, Magnetism and electronic structure of hcp Gd and the Gd (0001) surface, J. Phys. Condens. Matter **14**, 6353 (2002).

[57] G. Zhang, T. Jenkins, M. Bennett, and Y. Bai, Manifestation of intra-atomic 5d6s-4f exchange coupling in photoexcited gadolinium, J. Phys. Condens. Matter **29**, 495807 (2017).

[58] I. Turek, J. Kudrnovský, V. Drchal, and P. Bruno, Exchange interactions, spin waves, and transition temperatures in itinerant magnets, Philos. Mag. **86**, 1713 (2006).

[59] Y. O. Kvashnin, O. Grånäs, I. Di Marco, M. I. Katsnelson, A. I. Lichtenstein, and O. Eriksson, Exchange parameters of strongly correlated materials: Extraction from spin-polarized density functional theory plus dynamical mean-field theory, Phys. Rev. B **91**, 125133 (2015).

[60] S. Dudarev and P. Derlet, A "magnetic" interatomic potential for molecular dynamics simulations, J. Phys. Condens. Matter **17**, 7097 (2005).

[61] P. D. Desai, Thermodynamic properties of iron and silicon, J. Phys. Chem. Ref. Data **15**, 967 (1986).

[62] H. H. Potter, The magneto-caloric effect and other magnetic phenomena in iron, Proc. R. Soc. A **146**, 362 (1934).

[63] T. Gottschall, K. P. Skokov, M. Fries, A. Taubel, I. Radulov, F. Scheibel, D. Benke, S. Riegg, and O. Gutfleisch, Making a cool choice: The materials library of magnetic refrigeration, Adv. Energy Mater. **9**, 1901322 (2019).

[64] M. Baskes and R. Johnson, Modified embedded atom potentials for HCP metals, Model. Simul. Mater. Sci. Eng. **2**, 147 (1994).

[65] L. T. Kong, Phonon dispersion measured directly from molecular dynamics simulations, Comput. Phys. Commun. **182**, 2201 (2011).

[66] D. C. Wallace, *Statistical Physics of Crystals and Liquids: A Guide to Highly Accurate Equations of State* (World Scientific, Singapore, 2002).

[67] J. Hui and P. B. Allen, Thermodynamics of anharmonic crystals with application to Nb, J. Phys. C **8**, 2923 (1975).

[68] T. Maeda, Unusual elastic properties of gadolinium and invar, J. Phys. Soc. Jpn. **30**, 375 (1971).

[69] M. Rosen, Elastic moduli and ultrasonic attenuation of gadolinium, terbium, dysprosium, holmium, and erbium from 4.2 to 300 °K, Phys. Rev. **174**, 504 (1968).

[70] P. Jacobsson and B. Sundqvist, Thermal conductivity and electrical resistivity of gadolinium as functions of pressure and temperature, Phys. Rev. B **40**, 9541 (1989).

[71] C. Glorieux, J. Thoen, G. Bednarz, M. A. White, and D. J. W. Geldart, Photoacoustic investigation of the temperature and magnetic-field dependence of the specific-heat capacity and thermal conductivity near the curie point of gadolinium, Phys. Rev. B **52**, 12770 (1995).